JACS
JOURNAL OF THE AMERICAN CHEMICAL SOCIETY

Article

pubs.acs.org/JACS

Water Distribution, Dynamics, and Interactions with Alzheimer's β-Amyloid Fibrils Investigated by Solid-State NMR

Tuo Wang,[†] Hyunil Jo,[‡] William F. DeGrado,[‡] and Mei Hong*[,†]

[†]Department of Chemistry, Massachusetts Institute of Technology, Cambridge, Massachusetts 02139, United States

[‡]Department of Pharmaceutical Chemistry and Institute for Neurodegenerative Diseases, University of California, San Francisco, San Francisco, California 94143, United States

Supporting Information

ABSTRACT: Water is essential for protein folding and assembly of amyloid fibrils. Internal water cavities have been proposed for several amyloid fibrils, but no direct structural and dynamical data have been reported on the water dynamics and site-specific interactions of water with the fibrils. Here we use solid-state NMR spectroscopy to investigate the water interactions of several Aβ40 fibrils. ^{1}H spectral lineshapes, T_2 relaxation times, and two-dimensional (2D) ^{1}H−^{13}C correlation spectra show that there are five distinct water pools: three are peptide-bound water, while two are highly dynamic water that can be assigned to interfibrillar water and bulk-like matrix water. All these water pools are associated with the fibrils on the nanometer scale. Water-transferred 2D correlation spectra allow us to map out residue-specific hydration and give evidence for the presence of a water pore in the center of the three-fold symmetric wild-type Aβ40 fibril. In comparison, the loop residues and the intramolecular strand−strand interface have low hydration, excluding the presence of significant water cavities in these regions. The Osaka Aβ40 mutant shows lower hydration and more immobilized water than wild-type Aβ40, indicating the influence of peptide structure on the dynamics and distribution of hydration water. Finally, the highly mobile interfibrillar and matrix water exchange with each other on the time scale of seconds, suggesting that fibril bundling separates these two water pools, and water molecules must diffuse along the fibril axis before exchanging between these two environments. These results provide insights and experimental constraints on the spatial distribution and dynamics of water pools in these amyloid fibrils.

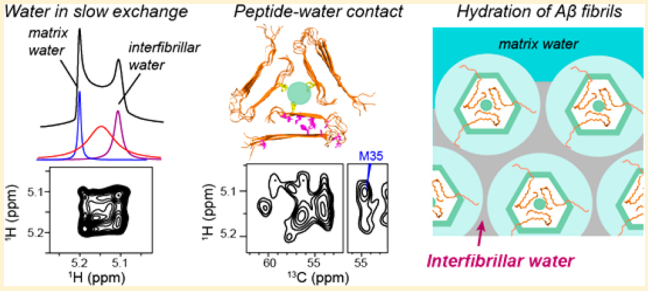

INTRODUCTION

Water plays a critical role in protein folding, function, and thermodynamic stability.[1,2] Solid-state NMR spectroscopy has been used extensively to investigate site-specific hydration of globular proteins,[3] membrane-bound proteins,[4−8] and biomolecular assemblies such as bacteriophages,[9] plant cell walls,[10,11] and bones.[12] In comparison, water interactions with amyloid fibrils, β-sheet-rich protein aggregates that occur in both functional proteins and pathologically misfolded proteins, have not been studied in detail. Early analysis of X-ray diffraction patterns of polyglutamine fibrils led to the proposal that many amyloids may be water-filled nanotubes,[13] but subsequent analysis of the diffraction patterns[14] and experimental data cast doubt on this conclusion. Instead, both anhydrous and water-encapsulating amyloids have been reported. For example, crystal structures of microcrystals formed by Gln- and Asn-rich peptides derived from the yeast prion Sup35p showed anhydrous steric-zipper interfaces, suggesting that the β-sheet structure may be entropically stabilized by exclusion of water.[15,16] However, to date, crystallographic structures have been limited to very short fragments of the full amyloid-forming region of proteins, hence primarily provide insight into the packing motifs that can be propagated in a crystal lattice, and presumably also within the most packed regions of a fibril. Application of high hydrostatic pressure to α-synuclein, a major component of the Lewy bodies of Parkinson's disease (PD),[17] caused fibril dissociation, suggesting that the hydrophobic core of the protein is dry until water is pushed into the core.[18,19] Dry and hydrated α-synuclein fibrils showed no NMR chemical shift differences, also suggesting an absence of internal water in these fibrils.[20] On the other hand, internal water cavities have been proposed for other amyloid fibrils. For example, comparison of the solid-state (SS)NMR determined structure of transthyretin fibrils with the reconstructed cryo-EM density maps led to the conclusion of large water cavities inside the fibrils, presumably hydrating the polar side chains.[21] X-ray fiber diffraction analysis has been conducted on three-fold symmetric fibrils formed by the Alzheimer's β-amyloid peptide (Aβ).[22] Comparison of the experimental equatorial diffraction intensities with the simulated patterns for various structural models led to the proposal that the three-fold fibrils contain a "hollow", water-filled, core at the trimer interface, which enlarged the volume of the original

Received: March 1, 2017
Published: April 13, 2017

DOI: 10.1021/jacs.7b02089
J. Am. Chem. Soc. 2017, 139, 6242−6252

solid-state NMR structural model.[23] Molecular dynamics (MD) simulations of Aβ(9−40) fibrils suggest that there may be multiple small internal hydration pockets in Aβ fibrils, which solvate a salt-bridge stabilized loop and the C-terminus.[24] Apart from these diffraction, microscopy, and simulation studies, direct site-specific experimental data about the spatial distribution, dynamics, and protein interactions of the hydration water of amyloid fibrils have not been reported.

In general, a complete description of the packing of amyloid fibrils requires consideration of a large number of potential water environments, each reflecting the hierarchic assembly of amyloid fibrils and each with distinct properties: (1) The most ordered waters are expected to play structural roles and help stabilize polar side chains within tightly packed regions of the fibril, similar to crystallographic waters within native proteins; (2) voids may occur within fibrils, e.g., near the central three-fold axis of Aβ fibrils; (3) protofibrils and fibrils assemble along partially or fully hydrated interfaces to form the morphologies seen by electron microscopy; (4) fibrils form hydrogels, which are expected to have large regions of water with properties approaching that of bulk water; and finally (5) amyloids such as those formed by τ and PrP have only a fraction of their sequences within the well-ordered amyloid, the remainder being either disordered or folded into small, poorly oriented folded domains. Aβ is noteworthy among proteins implicated in neurodegeneration in that the majority of its sequence lies within the amyloid-forming region, minimizing the contribution from extraneous domains that can complicate the understanding of the various classes of water.

We therefore investigated residue-specific water interactions with the fibrils formed by three Aβ peptides: wild-type (WT) Aβ40, the Osaka (E22Δ) mutant, and the Arctic (E22G) mutant.[25] Specifically, we probe the different types of water environments within a suspension of fibrils and examine whether water molecules associated with amyloid fibrils deviate significantly from waters of hydration seen in other biomolecules and whether the molecular structure differences among the Aβ40 subtypes correlate with differences in water dynamics and distribution. High-resolution structures of WT and Osaka Aβ40 fibrils have been determined, which provide a framework for describing the site-specific hydration of these assemblies. WT Aβ40 can exhibit at least three different molecular structures depending on the experimental conditions,[23,26,27] while the E22Δ mutant is monomorphic and has a different structure[28] from any of the WT Aβ40 polymorphs. The structure of Arctic Aβ40 is still unknown, and Arctic Aβ40 is highly polymorphic;[29] however, a recent chemical shift analysis[25] suggested that one of the main polymorphs of Arctic Aβ40 resembles WT Aβ42, whose high-resolution structure was determined recently.[30,31] In this study, we focus on the three-fold symmetric polymorph of the WT Aβ40 fibril and the monomorphic Osaka fibril. Using direct and indirect detection of water ^{1}H magic-angle spinning (MAS) NMR spectra and two-dimensional (2D) correlation experiments, we have identified five water pools associated with these fibrils. We present data on the volumes, dynamics, protein interactions, and spatial locations of these different water pools. Our data indicate that the hydration water of amyloid fibrils is more heterogeneous and has different macromolecular interactions from the hydration waters associated with lipid membranes, cell walls, and microcrystalline proteins. These differences reflect the unique molecular environments presented by the hierarchic assembly of amyloids and inform strategies for approaching the early detection and therapeutic intervention of protein misfolding diseases.

MATERIAL AND METHODS

Peptide Synthesis. ^{13}C, ^{15}N-labeled Aβ40 peptides were synthesized using a microwave peptide synthesizer (Alstra − Initiator, 0.2 mmol scale) with preloaded Chemmatrix-HMPB-Val resin (substitution level 0.5 mmol/g). Fmoc deprotection was performed by treatment with 0.1 M HOBt in 20% 4-methylpiperidine in DMF for 5 min at 70 °C. The coupling was performed twice with Fmoc amino acids (5 equiv), HCTU (4.98 equiv), and DIPEA (10 equiv) for 5 min at 75 °C. For ^{13}C, ^{15}N-labeled residues, labeled Fmoc amino acid (1.5 equiv), HCTU (1.49 equiv), and DIPEA (3 equiv) were used in the first coupling, while the second coupling was performed using unlabeled Fmoc amino acid (5 equiv), HCTU (4.98 equiv), and DIPEA (10 equiv). His residues were double-coupled at room temperature for 30 min, and Arg5 was triple-coupled. After coupling with Ala at residue 21, N-capping was performed with Ac_2O (10 equiv) and DIPEA (20 equiv) for 1 h. Cleavage was performed in a cocktail of TFA:TIPS:DTT (95:2.5:2.5) for 3 h, and the peptide was precipitated by cold ether and purified by reverse-phase HPLC using a Vydac C4 column at 60 °C. The fraction containing the desired peptide was pooled and lyophilized.

The Osaka and Arctic Aβ40 peptides contain ^{13}C, ^{15}N-labeled residues at F19, A21, I32, L34, V36, and G38.[25] Two WT Aβ40 peptides were synthesized. The first contains the same ^{13}C, ^{15}N-labeled residues as the Osaka and Arctic peptides, while the second peptide contains labeled residues at V12, F19, A21, V24, A30, I32, L34, and M35, giving a total of 10 labeled residues in this sequence.

Fibrillization. A purified and lyophilized peptide was dissolved in HFIP (5 mg/mL). 40 μL of this peptide solution was transferred to a 1.5 mL polypropylene eppendorf tube (VWR 87003-29t4) using a glass syringe. A total of 20 tubes were prepared in this way for 4 mg of lyophilized peptide to ensure that each tube contains 0.2 mg of Aβ40. HFIP was then removed by evaporation overnight, and residual solvent was further removed by Speedvac for 30 min. The peptide film in the tube was diluted with 20 μL of DMSO via a glass syringe to make a 10 mg/mL solution. The solution was briefly vortexed for 5−10 s and sonicated in a water bath for 5 min. Four or five tubes were sonicated in one batch, and each tube was mixed with 980 μL of 10 mM sodium phosphate buffer (pH = 7.2) and slowly pipetted 2−3 times to ensure mixing. The tube was then placed in the shaker at 37 °C, 900 rpm for 72−74 h. After shaking, the tube contents were carefully removed by pipet and transferred to a polycarbonate thick-wall centrifuge tube. A small amount (100−200 μL) of fresh buffer was used to transfer the residual fibril in the eppendorf tube. Each thick-wall centrifuge tube contains the contents from two eppendorf tubes. The samples were ultracentrifuged at 95,000 rpm for 1 h at 4 °C, giving clearly visible fibrils as opaque pellets. The supernatant was removed by a syringe, and the fibril solution from another two eppendorf tubes was added to the same tube and spun at 95,000 rpm for 1 h at 4 °C. The supernatant was again discarded by a syringe. The pellet was suspended in a small amount of phosphate buffer (500 μL), and the suspension was combined into an eppendorf tube by a pipet. The suspension in the eppendorf tube was spun again at 16,100 RCF for 1 h at 4 °C, and the supernatant was removed using a syringe to obtain the pellet.

Solid-State NMR Spectroscopy. Hydrated Aβ40 fibrils in the form of homogeneous translucent gels were centrifuged into 3.2 mm MAS rotors. All fibrils contain excess water relative to the peptide mass. We quantified the peptide and water masses of the samples by comparing the ^{1}H and ^{13}C spectral intensities together with gravimetric measurement of one of the fibrils after full lyophilization. Multiple WT Aβ40 samples were prepared, and all have hydration levels in a narrow range of 80−84% (w/w). The Osaka and Arctic Aβ40 fibrils have moderately lower hydrations of 64% and 74%, respectively. Direct inspection after spinning the samples at 10.5 kHz for extended periods of time indicates that there is no separate pool of supernatant water in the middle of the MAS rotors. Thus, at the

DOI: 10.1021/jacs.7b02089
J. Am. Chem. Soc. 2017, 139, 6242−6252

hydration levels and MAS frequencies used in this study, water is well mixed with the fibrils and does not separate under the centrifugal force of MAS.

Most solid-state NMR spectra were measured on a Bruker Avance II 800 MHz (18.8 T) spectrometer using a 3.2 mm triple-resonance HCN probe. Typical radiofrequency (rf) field strengths were 50−71 kHz for ^{1}H, 50−63 kHz for ^{13}C, and 36 kHz for ^{15}N. 0.5 mg DSS was added to the samples to allow water ^{1}H chemical shifts to be referenced internally to the DSS signal at 0 ppm. ^{13}C chemical shifts were externally referenced to the adamantane CH_2 signal at 40.48 ppm on the DSS scale. ^{15}N chemical shifts were externally referenced to the Met amide signal (127.88 ppm) of *N*-formyl-Met-Leu-Phe-OH[32] on the liquid ammonia scale. For variable-temperature 1D ^{1}H MAS experiments, all samples were equilibrated for at least 20 min between different temperatures. Long recycle delays of 4−10 s were used to minimize heating by radiofrequency pulses. The sample temperatures indicated here are thermocouple-reported values, which refer to the bearing gas temperature. At the MAS frequency of 10.5 kHz used in this work, the actual sample temperature is about 5 K higher than the thermocouple-reported values, as shown by the fact that at the thermocouple-reported temperature of 298 K, the water ^{1}H chemical shift corresponds to a sample temperature of 303 K based on the equation $\delta(H_2O) = 7.83 - T/96.9$ ppm.[33] At low temperatures, the same temperature differential is expected, although the water ^{1}H lineshapes broaden and become more complex, so that the equation cannot be used to estimate the sample temperature.

1D ^{1}H MAS spectra of hydrated Aβ40 fibrils were measured from 298 to 255 K under 10.5 kHz MAS. The spectra were deconvoluted using Dmfit.[34] 1D ^{1}H MAS spectra were also measured for several nonfibril samples as controls. A POPC membrane containing the transmembrane peptide of the parainfluenza virus 5 (PIV5) fusion protein F[35] was measured at 263 K on the 800 MHz spectrometer. A *Brachypodium* cell wall sample[36] was measured at 263 K on a 600 MHz spectrometer.

Directly detected ^{1}H T_2 relaxation times were measured using a Hahn echo experiment[8] with total echo delays of 0 to 280 ms. ^{13}C-detected ^{1}H T_2 relaxation was measured by adding a 1 ms ^{1}H−^{13}C Hartmann−Hahn cross-polarization (CP) step after the ^{1}H Hahn echo period (Figure S1a). All relaxation data were fit using a single exponential function.

2D ^{1}H−^{1}H exchange experiments were conducted at 263 K with ^{1}H mixing times of 0.1, 1.0, and 2.2 s and recycle delays of 4−10 s. 2D ^{1}H−^{13}C heteronuclear correlation (HETCOR) experiments[8,37] were conducted to probe site-specific water interactions of the Aβ fibrils (Figure S1b). A ^{1}H T_2 filter was first applied to suppress the peptide ^{1}H magnetization. The filter times were 0.57 ms × 2 for the WT peptide and 0.29 ms × 2 for the Osaka peptide. Water ^{1}H chemical shift was then encoded during the t_1 evolution period, after which the magnetization was transferred to peptide protons during a *z*-mixing period. The ^{1}H mixing times were 4 ms and 1.0 s to measure the chemical shifts of closely peptide-associated water versus remote water, respectively. After the ^{1}H mixing period, a 1 ms ^{1}H−^{13}C CP step allows detection of the ^{13}C chemical shifts to provide site-resolved information about the water environments.

To determine the water accessibilities of peptide residues with site resolution, we measured water-edited 2D ^{13}C−^{13}C and ^{15}N−^{13}C correlation spectra of WT Aβ40 fibrils at 263 K under 10.5 kHz.[38−40] The experiment used a ^{1}H T_2 filter of 0.57 ms × 2, followed by a short ^{1}H−^{1}H mixing period of 1.5 and 0.5 ms ^{1}H−^{13}C Lee−Goldburg CP (Figure S1c,d). The latter two conditions were chosen to minimize ^{1}H spin diffusion and maximize site-specificity of the detected water contact with the peptide residues. A control 2D spectrum with full intensities was measured without the ^{1}H T_2 filter but with the same ^{1}H−^{1}H mixing time as the water-edited spectra. Most residues in WT Aβ40 fibrils retained <4% of the intensities under these conditions, thus requiring a large number of scans, 1536 and 3712, for the water-edited ^{13}C−^{13}C and ^{15}N−^{13}C correlation experiments, respectively.

RESULTS

Temperature-Dependent ^{1}H Spectra Reveal Multiple Water Pools in Aβ40 Fibrils. We measured the ^{1}H spectra of WT, Osaka (E22Δ), and Arctic (E22G) Aβ40 fibrils as a function of temperature from 298 to 255 K (Figure 1). At 298 K, all three samples show a single water peak at 4.7 ppm. Interestingly, with decreasing temperature, the single water ^{1}H peak splits into two sharp peaks that sandwich a broad component. These multiple water peaks are observed between 278 and 263 K and indicate multiple water pools in slow exchange. At 278 K, all three Aβ fibrils show the two narrow peaks at ∼5.00 ppm and ∼4.95 ppm. The downfield displacement of the ^{1}H peaks with decreasing temperature is consistent with the known water ^{1}H chemical shift trend with increasing hydrogen bonding.[33] The temperature dependence of the 5.00 ppm peak (at 278 K) is larger than that of the 4.95 ppm peak, and the ^{1}H T_2 relaxation times are also longer (*vide infra*), indicating that the downfield signal corresponds to more mobile water. The integrated water intensity is constant from 298 to 263 K for the WT and Osaka Aβ40 fibrils, but at 255 K, the water signals broaden to a single peak with a 0.5 ppm line width, whose integrated intensity represents only 7−17% of the high-temperature intensity. Thus, the majority of water is frozen by 255 K, leaving only a small percentage of water that

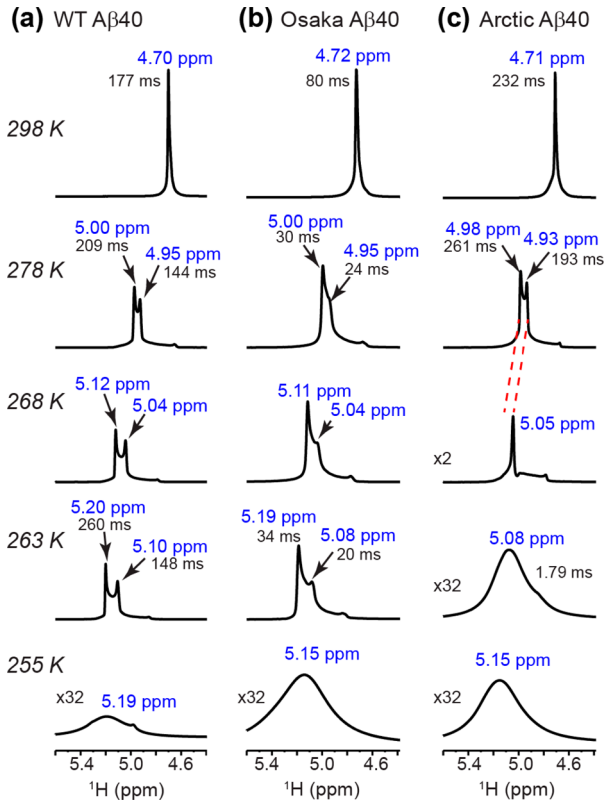

Figure 1. ^{1}H MAS spectra of water associated with (a) WT Aβ40, (b) Osaka Aβ40, and (c) Arctic Aβ40 fibrils as a function of temperature. The ^{1}H chemical shifts and ^{1}H-detected T_2 relaxation times are indicated. Red dashed lines in the Arctic Aβ40 spectra indicate the expected chemical shift change of the two sharp water peaks with decreasing temperature. A small peak that is ∼0.35 ppm upfield from the highest water peak is due to residual magnetic field inhomogeneity and is not considered further.

DOI: 10.1021/jacs.7b02089
J. Am. Chem. Soc. 2017, 139, 6242−6252

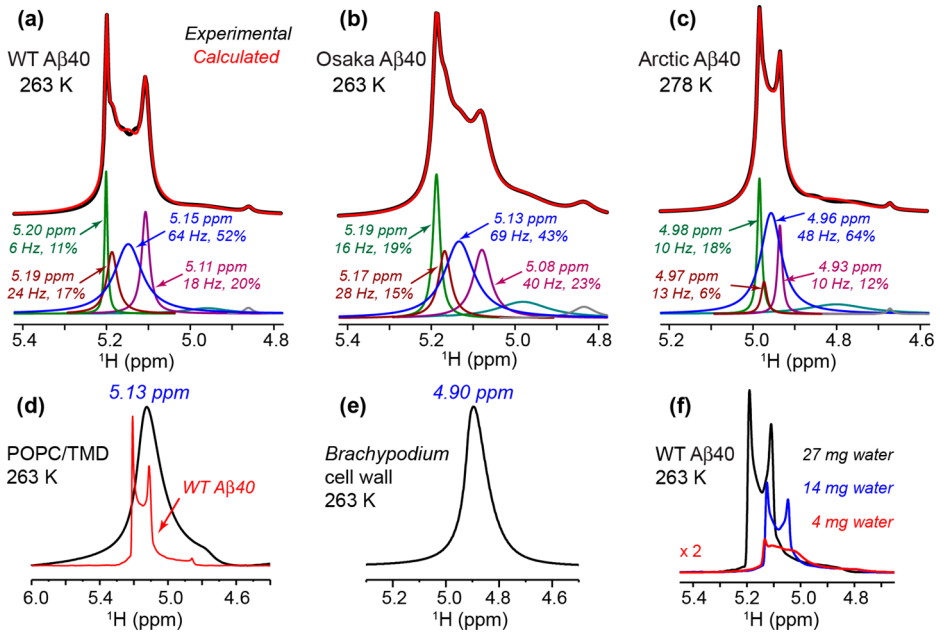

Figure 2. Comparison of the water ^{1}H MAS spectra of hydrated amyloid fibrils (a–c, f) and other systems (d, e). (a) WT Aβ40 fibrils. (b) Osaka Aβ fibrils. (c) Arctic Aβ40 fibrils. Fine features in the water peaks are resolved by deconvolution to give the ^{1}H chemical shifts, intensity fractions, and apparent line widths of each component (Table 1). (d) Water ^{1}H signals of POPC membranes containing the TMD of the parainfluenza virus 5 fusion protein at 263 K. The WT Aβ40 water ^{1}H spectrum is overlaid for comparison. (e) Water ^{1}H spectrum of *Brachypodium* cell walls. (f) Water ^{1}H spectra of Aβ40 fibrils at various hydration levels. The peptide mass is 5 mg.

Table 1. Water ^{1}H Chemical Shifts, Line Widths, and Populations from ^{1}H MAS Spectra of Aβ40 Fibrils[a]

peptide	δ_{1H} (ppm)	Area	FWHM (Hz)	^{1}H T_2 (ms)	Δ (Hz)	assignment
WT Aβ, 263 K	5.20, 5.19	11%, 17%	6.4, 24	260 ± 16	1.2	matrix[b]
	5.15	52%	64	93 ± 8	3.4	peptide-bound[c]
	5.11	20%	18	148 ± 10	2.2	interfibrillar
Osaka Aβ40, 263 K	5.19, 5.17	19%, 15%	16, 28	34 ± 1	9.4	matrix[b]
	5.13	43%	69	22 ± 2	14	peptide-bound[c]
	5.08	23%	40	20 ± 1	16	interfibrillar
Arctic Aβ40, 278 K	4.98, 4.97	18%, 6%	10, 13	261 ± 13	1.2	matrix[b]
	4.96	64%	48	116 ± 12	2.7	peptide-bound[c]
	4.93	12%	10	193 ± 11	1.6	interfibrillar

[a]The apparent line widths (FWHM) and populations are obtained by spectral deconvolution. ^{1}H-detected T_2 relaxation times yield the homogeneous line widths Δ according to $\Delta = 1/\pi T_2$. [b]Two components are needed to fit the downfield water peak. [c]The peptide-bound water includes both tightly and loosely bound water.

experiences significant freezing-point depression due to tight association with the peptide.[41,42]

^{1}H spin echo experiments indicate that the water associated with the Osaka Aβ40 fibril has 6–9-fold shorter ^{1}H T_2 relaxation times than the hydration water for WT and Arctic Aβ fibrils, indicating that water interaction with the Osaka Aβ is stronger than with the two other fibrils. This is consistent with the recently observed more rapid polarization transfer from water to Osaka peptide than to the other Aβ peptides.[25] The water ^{1}H T_2 relaxation times are relatively constant between 278 and 263 K for the WT and the Osaka Aβ fibrils, indicating small activation energies of water rotational diffusion. In comparison, the Arctic Aβ40 fibrils show different water dynamics: The downfield 5.0 ppm peak at 278 K is broadened beyond detection below 268 K, indicating that this mobile water component has a larger activation energy than in the other fibrils. The 4.93 ppm water peak persisted to 268 K but broadened by 263 K. Thus, the energetics of the water reorientational motion differs for different water pools within each fibril as well as for water associated with different fibrils.

To quantify the relative amounts of the various water pools, we analyzed in detail the "double-horn" ^{1}H spectra at 263 K for WT and Osaka Aβ fibrils and at 278 K for the Arctic Aβ fibrils. Spectral deconvolution confirms that the two sharp water peaks indeed sandwich a central broad resonance (Figure 2a). This central component resonates at 5.15 ppm for WT Aβ40, has a full width at half-maximum (FWHM) of 64 Hz, and represents 52% of the total spectral intensity (Table 1). The two mutants exhibit a similar broad water peak. We assign this broad water peak to peptide-associated water, as verified below by 2D ^{1}H–^{13}C correlation spectra (Figure 4). Comparison of the apparent ^{1}H line widths with the echo-detected homogeneous line widths indicates that all water peaks are inhomogeneously broadened (Table 1).

The "double-horn" patterns of the water ^{1}H MAS spectra of these fibrils are unusual, since hydrated lipid membranes and many other biomolecular assemblies typically exhibit either a

DOI: 10.1021/jacs.7b02089
J. Am. Chem. Soc. 2017, 139, 6242–6252

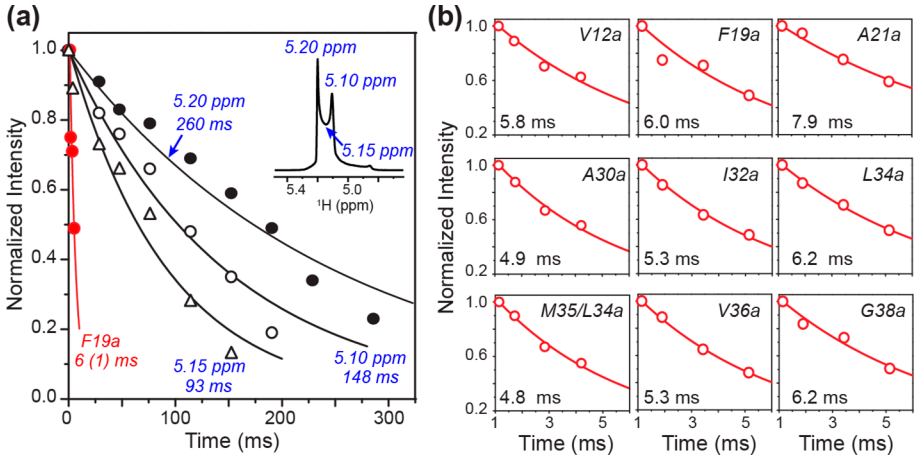

Figure 3. Representative ^{1}H-detected and ^{13}C-detected water T_2 relaxation time of WT Aβ40 fibrils at 263 K under 10.5 kHz MAS. (a) ^{1}H-detected water ^{1}H T_2 relaxation decays and best-fit relaxation times. The ^{13}C-detected ^{1}H T_2 decay of F19a is shown for comparison (red). (b) ^{13}C-detected ^{1}H T_2 relaxation decays of several Cα sites. A ^{1}H–^{1}H mixing time of 4 ms was used for all the measurements.

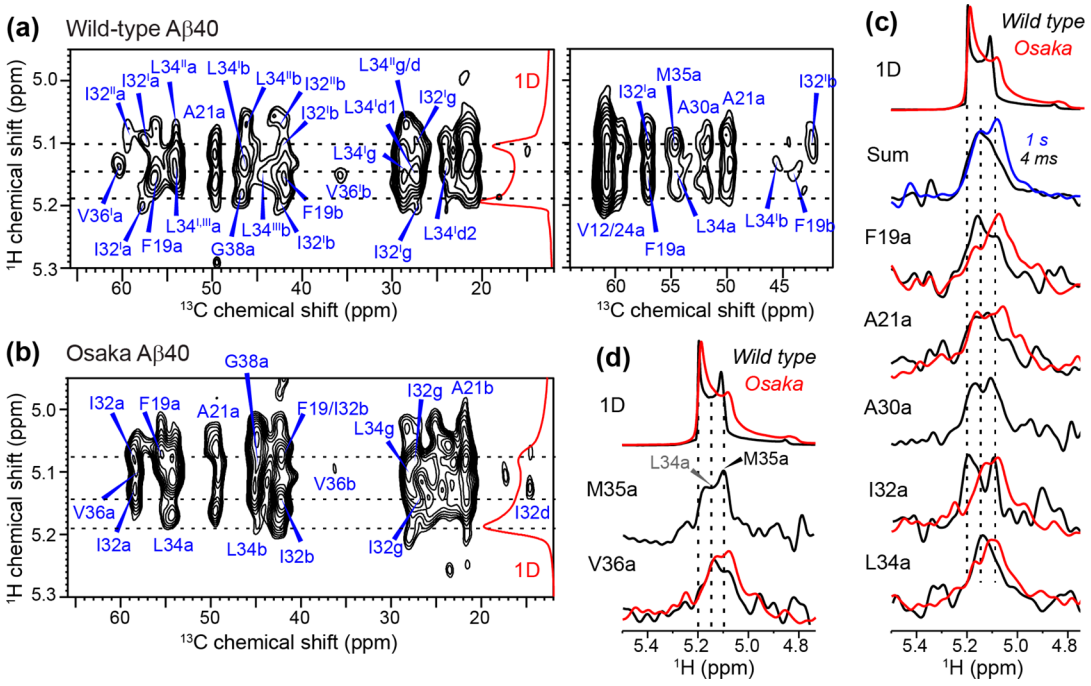

Figure 4. Site-specific water interactions of amyloid fibrils from 2D ^{1}H–^{13}C correlation spectra of (a) WT and (b) Osaka Aβ40 at 263 K. The spectra were measured with 4 ms ^{1}H–^{1}H mixing time (c, d) ^{1}H cross sections for various residues in WT (black) and Osaka (red) Aβ40 fibrils extracted from the 4 ms 2D HETCOR spectra. The ^{1}H projections of the 4 ms 2D spectrum (black) are compared with the ^{1}H projection of the 1.0 s 2D spectrum (blue), which shows a 5.10 ppm cross peak, indicating exchange with interfibrillar water.

single water ^{1}H peak or two resolved peaks with drastically different line widths. To illustrate the former case, Figure 2d,e shows representative water ^{1}H MAS spectra of a phospholipid membrane and a plant cell wall at 263 K. The membrane sample[35] shows a single water ^{1}H peak with a line width of 0.18 ppm, which spans the range of the multiple water peaks of the Aβ fibrils (Figure 2d), while the *Brachypodium* cell wall sample exhibits a single water ^{1}H peak with a 0.10 ppm line width, similar to other plant cell walls.[10,36] For cases where two water peaks have been resolved, the sharp upfield ^{1}H signal can be readily assigned to supernatant water that is separated from the protein by centrifugal forces under MAS, while the broad downfield ^{1}H peak can be assigned to protein-bound water.[9,33] To determine if one or both sharp peaks in the Aβ fibrils' water ^{1}H spectra results from such supernatant water, we reduced the hydration level of one of the fibril samples from 5-fold excess to 3-fold excess water and found the same ^{1}H spectral line shape, indicating that no water can be easily separated from the peptide (Figure 2f). This is consistent with the fact that the Osaka and Arctic fibrils show similar double-horn water ^{1}H spectra even though they contain less water (2- and 3-fold excess) than the WT sample (4- to 5-fold excess water). Only when the water mass is reduced to be comparable to the peptide mass does the ^{1}H spectrum change qualitatively, with the intensities of both sharp peaks decreasing significantly. Therefore, all water in these fibril samples are well associated with the peptides on the nanometer scale and cannot be separated by centrifugal forces under the MAS frequencies used

DOI: 10.1021/jacs.7b02089
J. Am. Chem. Soc. 2017, 139, 6242–6252

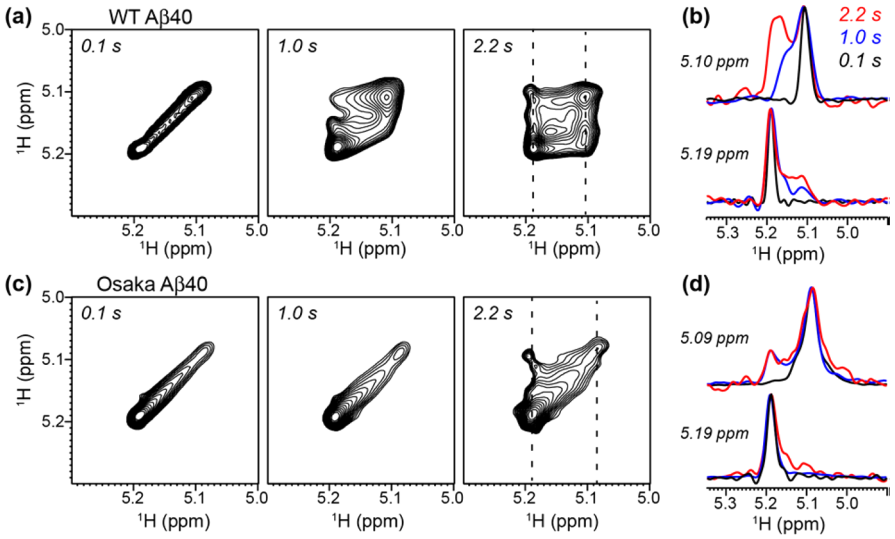

Figure 5. 2D $^{1}H-^{1}H$ MAS exchange spectra of (a) WT Aβ40 and (c) Osaka Aβ40 fibrils as a function of ^{1}H mixing time at 263 K. The ω_1 cross sections of the two sharp peaks (dashed lines) are extracted in (b) and (d). All 2D spectra are plotted using a minimum level that is 10% of the highest peak, a level increment of 1.15 and 16 contour levels. The spectra were measured at 10.5 kHz MAS.

here. This is consistent with visual inspection of the samples after extended periods of MAS, which found no separate water pool in the middle of the rotor, unlike water of microcrystalline proteins.

Multiple Water Pools Have Distinct Relaxation Times. ^{1}H T_2 relaxation times give insight into the dynamics of water in the different environments (Figure 3). At 263 K for the WT sample, the ^{1}H T_2 is the longest for the 5.20 ppm peak (260 ms), intermediate for the 5.10 ppm peak (150 ms), and the shortest for the 5.15 ppm peak (93 ms) (Figure 3a), suggesting that peptide−water interactions increase in the order of 5.20, 5.10, and 5.15 ppm. To detect the ^{1}H T_2 of water molecules that are adjacent to the peptide, we measured T_2 through ^{13}C detection, by adding a 4 ms ^{1}H mixing period and a 1 ms $^{1}H-^{13}C$ CP step after the ^{1}H spin−echo period (Figure S1a).[37] The resulting Cα-detected water ^{1}H T_2's range from 5 to 8 ms (Figure 3b), which are an order of magnitude shorter than the ^{1}H detected T_2 values. These short water ^{1}H T_2 relaxation times indicate that some water molecules directly interact with and are significantly immobilized by the peptide. These tightly bound water molecules likely give rise to the substantial freezing-point depression (Figure 1). For all labeled residues between V12 and G38 in WT Aβ40, the ^{13}C-detected ^{1}H T_2 values are relatively uniform, indicating no significant dynamical gradient of the bound water molecules along the two β-strands. Together, these relaxation data resolved four dynamically distinct water pools, with ^{1}H T_2 relaxation times ranging from 260 to 5 ms. The Arctic mutant has very similar water ^{1}H T_2's as the WT peptide, while the Osaka peptide has significantly shorter T_2's.

$^{1}H-^{13}C$ 2D Correlation Spectra Reveal Site-Specific Water−Peptide Interactions. To determine residue-specific hydration, we measured 2D $^{1}H-^{13}C$ correlation spectra of WT and Osaka Aβ40 at 263 K. After ^{1}H chemical shift encoding in t_1, a ^{1}H mixing time of 4 ms was used before cross-polarization to ^{13}C for detection (Figure S1b). Unexpectedly, these fibrils exhibit several resolved water ^{1}H frequencies even for closely spaced residues. Within a small ^{1}H spectral range of 0.10 ppm, at least three ^{1}H chemical shifts can be resolved (Figure 4a). This high water ^{1}H resolution stands in contrast to the water that hydrates membrane proteins and polysaccharide-rich cell walls[4,8,10] and indicates that water molecules associated with different residues of the peptide undergo slow exchange. For WT Aβ40, F19, L34, and V36 exhibit a predominant water correlation peak at 5.15 ppm, while A21, A30, and I32 exhibit two water cross peaks, suggesting a more heterogeneous water environment at the loop (Figure 4c,d). The ^{1}H projection of the 2D spectrum shows a maximum at 5.15 ppm, confirming the assignment of this chemical shift to peptide-bound water. The water ^{1}H chemical shifts differ between WT and Osaka fibrils for the same residues (Figure 4b). For example, F19 Cα shows a water cross peak at 5.15 ppm in the WT sample but 5.08 ppm in the Osaka Aβ fibril. I32 Cα correlates with two resolved water cross peaks (5.20 and 5.10 ppm) in WT Aβ40, while in the Osaka Aβ fibril I32 has a predominant water ^{1}H cross peak at 5.08 ppm. Thus, at the moderate low temperature used in these experiments, we can resolve distinct residue-specific water environments, and the water structure and dynamics are influenced by the molecular structures of the peptides.

Different Water Pools of WT Aβ40 Undergo Exchange on the Time Scale of Seconds. To gain insight into the locations and mutual interactions of the different water pools, we measured 2D $^{1}H-^{1}H$ exchange spectra of the WT and Osaka Aβ40 fibrils at 263 K (Figure 5). At the shortest ^{1}H mixing time of 0.1 s, both spectra show a diagonal ridge, confirming the inhomogeneous nature of the water peaks. With 1.0 and 2.2 s ^{1}H mixing, extensive cross peaks are observed for the WT fibrils. The cross peaks occur between all three water components, and by 2.2 s, the exchange is complete, exhibiting a square-like pattern (Figure 5a), indicating that both the dynamic water pools and the peptide-bound water are well mixed. The exchange occurs first between the 5.15 ppm peptide-bound water and the two narrow water peaks at 5.10 and 5.20 ppm, then between the two narrow peaks (Figure 5b). To confirm that the water that gives rise to the narrow peaks in the ^{1}H spectra is indeed in close proximity to the peptides, we measured a 2D $^{1}H-^{13}C$ correlation spectrum with a long ^{1}H mixing time of 1 s (Figure 4c). An additional ^{1}H cross peak appeared at 5.10 ppm, which was absent in the 4 ms 2D

DOI: 10.1021/jacs.7b02089
J. Am. Chem. Soc. 2017, 139, 6242−6252

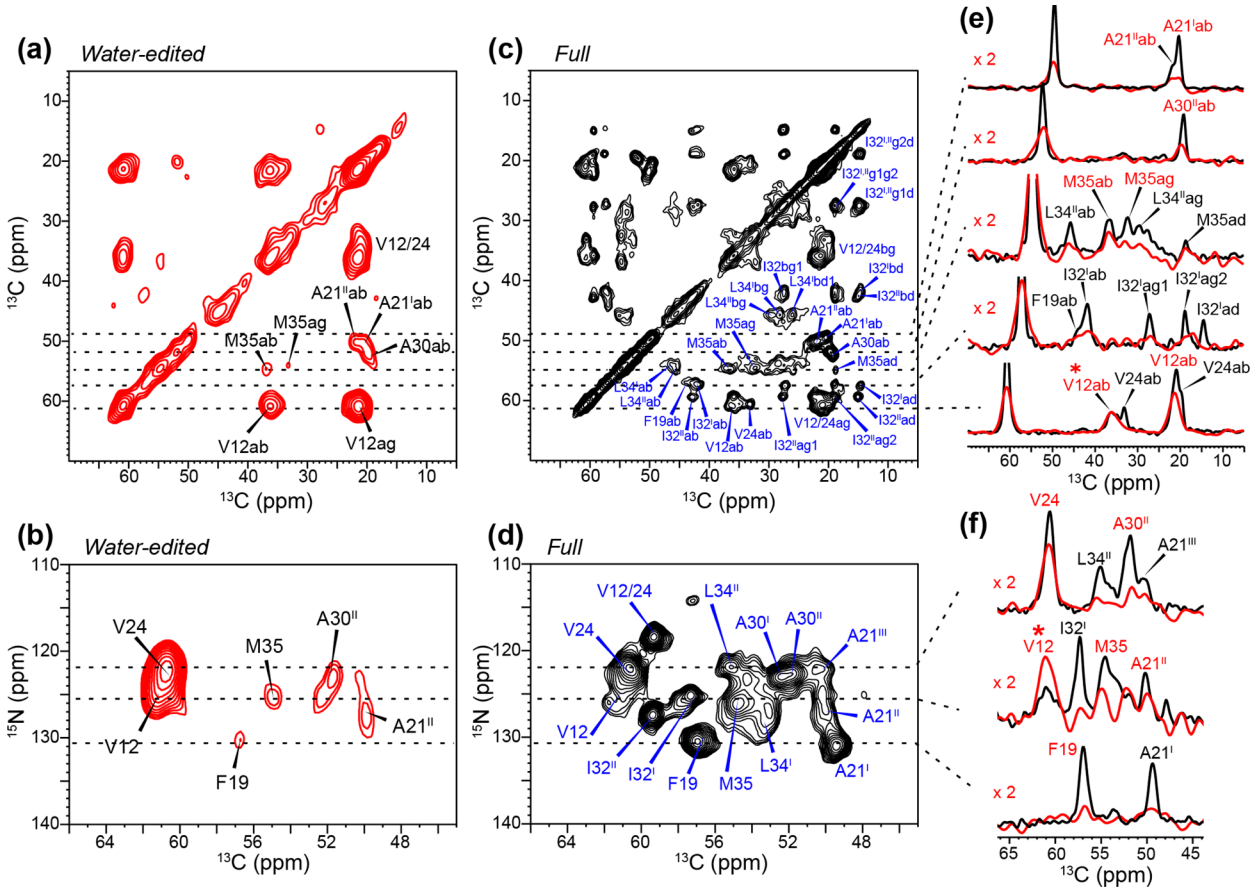

Figure 6. Water-edited 2D correlation spectra of WT Aβ40 fibrils. (a, b) Water-edited ^{13}C−^{13}C 50 ms DARR and ^{15}N−^{13}C correlation spectra. (c, d) Control ^{13}C−^{13}C 50 ms DARR and ^{15}N−^{13}C correlation spectra. Preferential retention of M35 cross peaks indicates the presence of a water cavity in the core of WT Aβ40 fibrils. (e, f) Representative ^{13}C cross sections from 2D water-edited (red) and control (black) spectra. The spectra were normalized by V12 signals (asterisk). The plotted cross sections are the sum of corresponding ω_1 and ω_2 cross sections for both control and water-edited 2D ^{13}C−^{13}C DARR spectra.

spectrum. Thus, the 5.15 ppm peptide-bound water indeed exchanges with the mobile water at 5.10 ppm. Compared to the WT fibrils, the Osaka Aβ40 fibrils show much weaker cross peak intensities, indicating that the water pools are more separated in this fibril.

Water-Edited 2D Correlation Spectra Indicate a Water-Filled Pore in the Center of the Three-Fold WT Aβ40 Fibrils. The multiple water ^{1}H correlation signals with the peptide in the 2D ^{1}H−^{13}C correlation spectra suggest that hydration levels may differ for different residues. To test this, we measured water-edited 2D ^{13}C−^{13}C and ^{15}N−^{13}C correlation spectra and compared them with control spectra with full intensities (Figure 6). A short ^{1}H mixing time of 1.5 ms and Lee−Goldburg CP were used to minimize ^{1}H spin diffusion and restrict our detection only to water that is closely associated with each residue. Out of the eight detected residues in the WT Aβ40 sample, V12 shows the highest residual Cα−Cβ and N−Cα cross peaks in the water-edited 2D spectra (Figure 6a, b), indicating that the unstructured N-terminal segment is the best hydrated segment of the peptide. For comparison, V24, which is resolved from the V12 signals in the 2D ^{15}N−^{13}C correlation spectrum, shows much weaker water-transferred intensity (Figure 6c), indicating low hydration of the interstrand loop. I32 and L34, which are located in the hydrophobic core of the peptide, also do not exhibit strong water-transferred intensities, indicating that the C-terminal β-strand is poorly hydrated. In contrast, M35, which has relatively weak cross peaks in the full-intensity control spectra, exhibits significant residual Cα−Cβ, Cα−Cγ, and N−Cα cross peaks in the water-edited 2D spectra.

Figure 7 quantifies the residual intensities of the water-edited spectra for different residues and different polymorphs of WT Aβ40. The intensity ratios between the water-edited and control spectra are normalized by the Cα−Cβ and Nα−Cα intensities of the best hydrated V12 (Table S1). V12 has the highest water-transferred intensities (63−100%), which are more than 2-fold higher than the intensities of other residues. The second highest water transfer is found for M35, with an average intensity of 32%. Since M35 side chain points to the center of the three-fold symmetric fibril, the hydration water must come from the center of the triangular fibril cross section, away from the hydrophobic β-strands. This is supported by the fact that residues adjacent to M35, including L34, I32, and A30, have much lower residual intensities of 18%, 11%, and 19%, respectively. Moreover, F19 and A21 on the N-terminal β-strand also show limited water-transferred intensities (24% and 20%). Taken together, these results indicate that the hydrophobic strand−loop−strand region of the WT peptide are relatively dry, in qualitative contrast to the well-hydrated disordered N-terminus and the center of the three-fold fibril.

DOI: 10.1021/jacs.7b02089
J. Am. Chem. Soc. 2017, 139, 6242−6252

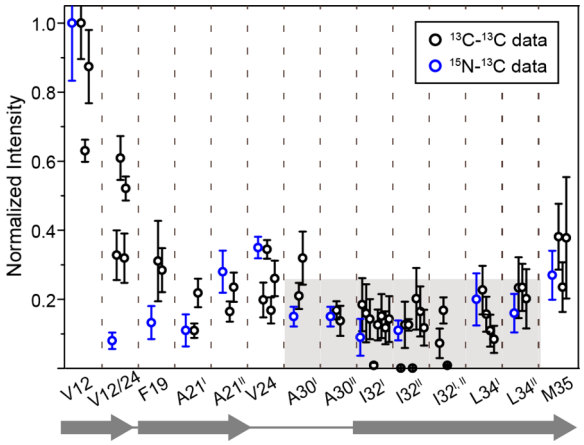

Figure 7. Site-specific relative intensities of water-edited peaks versus the full peaks from 2D ^{15}N−^{13}C (blue) and ^{13}C−^{13}C (black) spectra of WT Aβ40. The relative intensities between the water-edited and control spectra first normalized by the number of scans and then further normalized by the V12Cα−Cβ or V12Nα−Cα cross peaks. For each residue, the relative intensity of multiple ^{13}C−^{13}C cross peaks are compared between water-edited and control spectra. Several residues have two polymorphs as denoted using superscripts I and II. The relative intensities for different cross peaks are summarized in Table S1. The error bars are obtained from standard deviations of cross-peak intensities.

DISCUSSION

The above ^{1}H chemical shifts, T_2 relaxation times, and water−protein correlation data identified a total of five water pools in WT Aβ fibrils, indicating significant heterogeneity of the hydration water. The double-horn ^{1}H spectra of these fibrils at moderate low temperatures are not due to susceptibility effects or inhomogeneous magnetic fields, since high-temperature spectra show a narrow water peak, and exchange cross peaks are observed between the different water pools. The two narrow peaks of the fibril water are also not due to supernatant water, as seen for microcrystalline proteins and filamentous bacteriophages,[3,9,33] but are instead associated with the peptides based on 2D ^{1}H−^{13}C correlation spectra (Figure 4) and ^{1}H−^{1}H exchange spectra (Figure 5). The hydration water of these fibrils differs from water of other biomolecular mixtures such as lipid membranes and plant cell walls, which exhibit only a single averaged water ^{1}H frequency at the same temperature. Therefore, the hydration waters of Aβ fibrils are separated and trapped into multiple distinct chemical and physical environments, among which they exchange only on the time scale of seconds.

Figure 8 shows the assignment and the proposed model of the different water pools in the three-fold WT Aβ40 fibrils. All indicated T_2 relaxation times are for 263 K, and the indicated water fractions are obtained from ^{1}H spectral deconvolution. The hydration shells are depicted in approximate proportion to the volumes calculated based on the 80−84% hydration level of the WT Aβ40 fibrils. First, a small water pool is identified in the center of the three-fold WT fibril (Figure 8a), based on the high water accessibility of M35 seen in the water-edited 2D ^{13}C−^{13}C correlation spectra. This pore water has a ^{1}H chemical shift of 5.10 ppm (Figure 4a, d) and a T_2 relaxation time of ∼5 ms (Figure 3b). The molecular structure of the three-fold fibril indicates that the central pore occupies <10% of the total area of the fibril cross section,[23] which indicates that this pore water represents only about 1−2% of the total water at the hydration content of our samples.

The presence of a water pore at the trimer interface of the three-fold fibril is consistent with recent ^{2}H NMR data of *in vitro* WT Aβ40. These studies found that methyl motions of L17, L34, and L36 in the hydrophobic core are independent of fibril hydration, while M35 methyl motion is strongly dependent on the hydration level, with substantial line-narrowing in the wet state compared to the dry state.[43] Moreover, M35 motion at high temperatures in the hydrated fibrils contains a diffusive component in addition to the fast methyl three-site jumps.

The second type of water has ^{1}H chemical shifts of 5.05−5.20 ppm (peaked at 5.15 ppm), short ^{1}H T_2 relaxation times of 5−8 ms, and rapid polarization transfer (within 4 ms) to the peptide, thus we assign this to tightly peptide-bound water. The tightly bound water, together with pore water, experiences

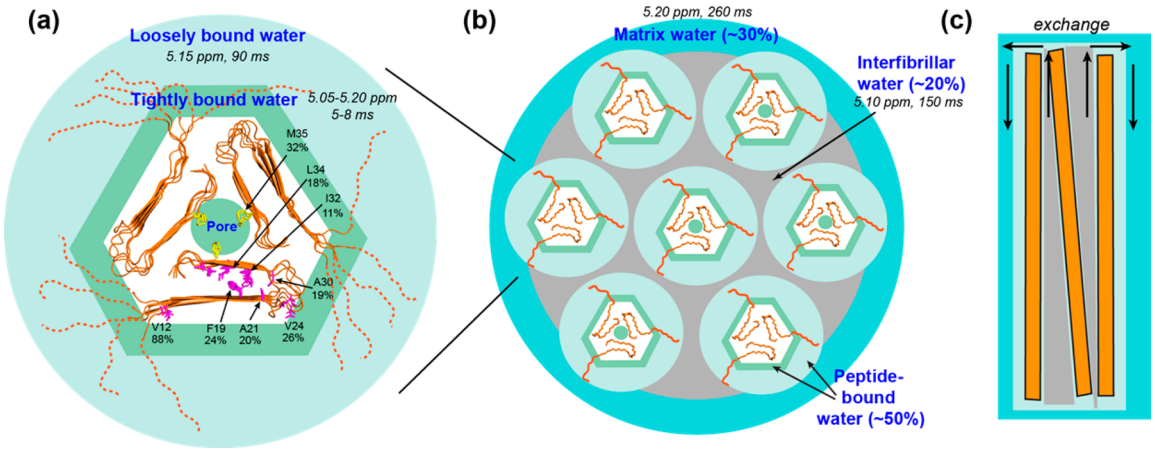

Figure 8. Schematic of the proposed multiple water pools associated with the three-fold WT Aβ40 fibrils. (a) Top view of the fibril with the unstructured N-terminus indicated as dashed lines. ^{13}C, ^{15}N-labeled residues are shown in sticks, and the average hydration percentage per residue is indicated. M35 (yellow) shows a high hydration level, supporting the presence of a central water cavity. The hydration shell formed by the tightly bound and loosely bound water has a diameter that is about two times larger than the fibril triangular side length. (b) Top view of several laterally associated three-fold fibrils, creating an interfibrillar water pool. The ^{1}H chemical shifts, ^{1}H T_2 relaxation times, and fraction of the various water pools are indicated. (c) Side view of three-fold WT Aβ40 fibrils (orange) and the associated water pools.

DOI: 10.1021/jacs.7b02089
J. Am. Chem. Soc. 2017, 139, 6242−6252

significant freezing point depression and accounts for ∼7% of the total water amount in our WT Aβ40 sample (Figure 1a, bottom). This provides a 2−3 nm-thick hydration shell. The third water pool has a similar ^{1}H chemical shift of 5.15 ppm but exhibits a much longer T_2 relaxation time of 90 ms, indicating higher mobility. We assign this component to loosely peptide-bound water, specifically interacting with the unstructured N-terminus. Together, the pore water, the tightly bound water, and the loosely bound water account for about half of the total water in the WT fibrils (Table 1). At the hydration content of these samples, this corresponds to a hydration shell of ∼14 nm total diameter, encompassing the triangular fibril with a side length of ∼7 nm (Figure 8a).

Previous MD simulations suggested that Aβ40 fibrils may contain multiple internal water cavities, including not only the pore at the center of the triangular fibril[22,44] but also the loop and the C-terminus.[24,45] The loop water is proposed to hydrate a D23-K28 salt bridge, which is present in a two-fold WT polymorph[27] but absent in the three-fold fibril. Our current data on the three-fold fibril show low hydration of residues between A21 and I32 (Figure 7), thus is consistent with this prediction. Our data indicate that the hydrophobic strand−loop−strand segment from F19 to V36 is poorly hydrated, with the exception of M35.

While the broad water resonance can be readily assigned to peptide-bound water, the two narrow water peaks that flank the peptide-bound water peak are more surprising. The upfield 5.10 ppm ^{1}H signal has a slightly lower population and corresponds to less dynamic water than the downfield 5.20 ppm peak. The 5.10 ppm water is also better associated with the peptide based on ^{1}H−^{13}C and ^{1}H−^{1}H correlation spectra. We assign the upfield peak to interfibrillar water and the downfield peak to bulk-like matrix water. The proposal of interfibrillar water is guided by transmission electron microscopy (TEM) images of these Aβ fibrils, which show regions with 3−4 laterally associated fibrils to give a total width of 50−60 nm (Figure S2).[25] The peptide concentrations in the NMR samples are about 3 orders of magnitude higher than those used for EM measurements (0.2 mg/mL), thus fibril bundling should be extensive. We propose that the water molecules between fibrils are responsible for the 5.10 ppm peak, and the relatively long T_2 relaxation time of 150 ms indicates that this interfacial water is highly dynamic. In comparison, the remaining ∼30% of water in the WT Aβ fibrils can be assigned to bulk-like matrix water, since it has the narrowest line width, the longest ^{1}H T_2 of 260 ms, and the weakest interaction with the peptide, requiring the longest time to exchange with the other water (Figure 8b, c). The preferential freezing of the downfield water peak in the Arctic Aβ sample, which is indicative of strong water−water hydrogen bonding, also supports the assignment of this downfield peak to bulk matrix water.

The 2D ^{1}H−^{1}H exchange spectra provide important insights into the nature of diffusion between the interfibrillar water and the bulk water. Complete exchange of the water pools of the WT Aβ40 fibrils is reached after ∼2 s, which is slow for water translational diffusion in most chemical systems. The self-diffusion coefficients of water are 10^{-6} cm^2/s at ambient temperature. Moderate cooling decreases this value by less than an order of magnitude,[46] consistent with the low activation energy of water translational diffusion. Interactions with organic polymers such as Nafion also do not slow down this diffusion significantly.[46] The fact that the 5.20 ppm and 5.10 ppm ^{1}H signals of the WT Aβ40 water have narrow homogeneous line widths of 1−2 Hz confirms the high mobility of water molecules in these environments. Thus, the exchange time scale of 1−2 s indicates a diffusion length scale of a few microns. Since our volume estimates and peptide-water correlation peaks indicate that the hydration shell that includes the peptide-bound water and interfibrillar water of a single fibril has a diameter of <∼20 nm, the micron diffusion length can only be explained by translational diffusion of the interfibrillar water along the fibril axis for microns before equilibrating with the bulk matrix water (Figure 8c). In other words, the two mobile water pools are compartmentalized by laterally aggregated fibrils and only exchange after traveling the length of the fibrils. This longitudinal water diffusion has some resemblance to the concept of water-filled nanotubes, where water was thought to exit and enter the fibril at the two ends. But our data suggest that the mobile water that manifests such exchange is sequestered between multiple fibrils instead of within each fibril.

Finally, we comment on the differences between hydration water of the Osaka Aβ40 fibrils and the WT fibrils. The Osaka Aβ40 structure differs substantially from the three-fold WT Aβ40 structure: The E22Δ mutant dimerizes into a rectangular cinnamon roll shape with a 6 × 3 nm dimension for the fibril cross section.[28] The N-terminal segment is well ordered, and the fibril interior is densely packed with hydrophobic side chains, with few detectable cavities for potential water permeation. Consistent with this more rigid and compact structure, the water associated with the Osaka fibrils has shorter ^{1}H T_2 relaxation times, and the T_2 decreases more rapidly with temperature (Figure 1), indicating higher activation energies of water motion. On the mesoscopic level, the interfibrillar water has limited exchange with the bulk matrix water (Figure 5), indicating a more complete separation of the two water pools. Based on the populations of the different water pools of the Osaka fibril (Figure 2) and the total water content of this sample, we estimate that the hydration shell of the Osaka fibril has a dimension of about 8 × 4 nm, which is much smaller than the hydration shell of the three-fold WT fibrils.

CONCLUSIONS

The ^{1}H and ^{13}C solid-state NMR data shown here distinguished five water pools in WT Aβ40 fibrils, as characterized by different ^{1}H chemical shifts, T_2 relaxation times, peptide interactions, and spatial locations. All water pools are well mixed with the peptides and cannot be phase-separated under moderate MAS and at moderate low temperature. Thus, water interacts with these fibrils more strongly than with globular proteins and lipid membranes. For the WT three-fold Aβ40 fibrils, water−protein correlation spectra indicate the presence of a long-proposed water pore at the trimer interface, but exclude significant water cavities at the loop and the two β-strands. The presence of a disordered N-terminus in the WT fibril and its absence in the Osaka Aβ40 fibril give rise to significantly different dynamics of peptide-bound water. Interestingly, for all three Aβ fibrils examined here, two highly mobile and spatially separate water pools are identified and can be assigned to water trapped between laterally associated fibrils and bulk-like matrix water. The mobile water in these two environments exchanges with each other on the time scale of seconds, indicating that the interfibrillar water travels the micron lengths of the fibrils before exchanging with external bulk water. These results indicate that amyloid fibrils, due to their morphology and

DOI: 10.1021/jacs.7b02089
J. Am. Chem. Soc. 2017, 139, 6242−6252

molecular structures, cause highly heterogeneous water environments that are uncommon for hydration water of other biomolecular assemblies. Since the dynamic interfibrillar water appears to be unique to these amyloid fibrils[47] and is absent in nonfibrous proteins, it may provide an opportunity for early detection of fibrillar aggregates in tissues using magnetic resonance imaging and for design of small-molecule drugs that target this region.

■ ASSOCIATED CONTENT

Supporting Information

The Supporting Information is available free of charge on the ACS Publications website at DOI: 10.1021/jacs.7b02089.

Table of water-transferred spectral intensities to quantify water accessibilities; summary of NMR pulse sequences for measuring water-amyloid interactions; and TEM images of Aβ40 showing lateral associations of fibrils (PDF)

■ AUTHOR INFORMATION

Corresponding Author

*meihong@mit.edu

ORCID

Tuo Wang: 0000-0002-1801-924X

Mei Hong: 0000-0001-5255-5858

Notes

The authors declare no competing financial interest.

■ ACKNOWLEDGMENTS

This work is supported by National Institutes of Health grants GM066976 and P01 AG002132.

■ REFERENCES

(1) Halle, B. *Philos. Trans. R. Soc., B* **2004**, *359*, 1207−1223.
(2) Nakasako, M. *Philos. Trans. R. Soc., B* **2004**, *359*, 1191−1204.
(3) Lesage, A.; Bockmann, A. *J. Am. Chem. Soc.* **2003**, *125*, 13336−13337.
(4) Luo, W.; Hong, M. *J. Am. Chem. Soc.* **2010**, *132*, 2378−2384.
(5) Ader, C.; Schneider, R.; Seidel, K.; Etzkorn, M.; Becker, S.; Baldus, M. *J. Am. Chem. Soc.* **2009**, *131*, 170−176.
(6) Weingarth, M.; van der Cruijsen, E. A.; Ostmeyer, J.; Lievestro, S.; Roux, B.; Baldus, M. *J. Am. Chem. Soc.* **2014**, *136*, 2000−2007.
(7) Shi, L.; Kawamura, I.; Jung, K. H.; Brown, L. S.; Ladizhansky, V. *Angew. Chem., Int. Ed.* **2011**, *50*, 1302−1305.
(8) Williams, J. K.; Hong, M. *J. Magn. Reson.* **2014**, *247*, 118−127.
(9) Sergeyev, I. V.; Bahri, S.; Day, L. A.; McDermott, A. E. *J. Chem. Phys.* **2014**, *141*, 22D533.
(10) White, P. B.; Wang, T.; Park, Y. B.; Cosgrove, D. J.; Hong, M. *J. Am. Chem. Soc.* **2014**, *136*, 10399−10409.
(11) Wang, T.; Park, Y. B.; Cosgrove, D. J.; Hong, M. *Plant Physiol.* **2015**, *168*, 871−84.
(12) Wilson, E. E.; Awonusi, A.; Morris, M. D.; Kohn, D. H.; Tecklenburg, M. M.; Beck, L. W. *Biophys. J.* **2006**, *90*, 3722−31.
(13) Perutz, M. F.; Finch, J. T.; Berriman, J.; Lesk, A. *Proc. Natl. Acad. Sci. U. S. A.* **2002**, *99*, 5591.
(14) Jahn, T. R.; Makin, O. S.; Morris, K. L.; Marshall, K. E.; Tian, P.; Sikorski, P.; Serpell, L. C. *J. Mol. Biol.* **2010**, *395*, 717−727.
(15) Balbirnie, M.; Grothe, R.; Eisenberg, D. S. *Proc. Natl. Acad. Sci. U. S. A.* **2001**, *98*, 2375−2380.
(16) Nelson, R.; Sawaya, M. R.; Balbirnie, M.; Madsen, A. Ø.; Riekel, C.; Grothe, R.; Eisenberg, D. *Nature* **2005**, *435*, 773−778.
(17) Spillantini, M. G.; Schmidt, M. L.; Lee, V. M.; Trojanowski, J. Q.; Jakes, R.; Goedert, M. *Nature* **1997**, *388*, 839−840.
(18) de Oliveira, G. A.; Marques, M. A.; Cruzeiro-Silva, C.; Cordeiro, Y.; Schuabb, C.; Moraes, A. H.; Winter, R.; Oschkinat, H.; Foguel, D.; Freitas, M. S.; Silva, J. L. *Sci. Rep.* **2016**, *6*, 37990.
(19) Tuttle, M. D.; Comellas, G.; Nieuwkoop, A. J.; Covell, D. J.; Berthold, D. A.; Kloepper, K. D.; Courtney, J. M.; Kim, J. K.; Barclay, A. M.; Kendall, A.; Wan, W.; Stubbs, G.; Schwieters, C. D.; Lee, V. M.; George, J. M.; Rienstra, C. M. *Nat. Struct. Mol. Biol.* **2016**, *23*, 409−415.
(20) Kloepper, K. D.; Hartman, K. L.; Ladror, D. T.; Rienstra, C. M. *J. Phys. Chem. B* **2007**, *111*, 13353−13356.
(21) Fitzpatrick, A. W.; Debelouchina, G. T.; Bayro, M. J.; Clare, D. K.; Caporini, M. A.; Bajaj, V. S.; Jaroniec, C. P.; Wang, L.; Ladizhansky, V.; Muller, S. A.; MacPhee, C. E.; Waudby, C. A.; Mott, H. R.; De Simone, A.; Knowles, T. P.; Saibil, H. R.; Vendruscolo, M.; Orlova, E. V.; Griffin, R. G.; Dobson, C. M. *Proc. Natl. Acad. Sci. U. S. A.* **2013**, *110*, 5468−5473.
(22) McDonald, M.; Box, H.; Bian, W.; Kendall, A.; Tycko, R.; Stubbs, G. *J. Mol. Biol.* **2012**, *423*, 454−61.
(23) Paravastu, A. K.; Leapman, R. D.; Yau, W. M.; Tycko, R. *Proc. Natl. Acad. Sci. U. S. A.* **2008**, *105*, 18349−54.
(24) Buchete, N. V.; Tycko, R.; Hummer, G. *J. Mol. Biol.* **2005**, *353*, 804−21.
(25) Elkins, M. R.; Wang, T.; Nick, M.; Jo, H.; Lemmin, T.; Prusiner, S. B.; DeGrado, W. F.; Stöhr, J.; Hong, M. *J. Am. Chem. Soc.* **2016**, *138*, 9840−9852.
(26) Bertini, I.; Gonnelli, L.; Luchinat, C.; Mao, J. F.; Nesi, A. *J. Am. Chem. Soc.* **2011**, *133*, 16013−16022.
(27) Petkova, A. T.; Yau, W. M.; Tycko, R. *Biochemistry* **2006**, *45*, 498−512.
(28) Schutz, A. K.; Vagt, T.; Huber, M.; Ovchinnikova, O. Y.; Cadalbert, R.; Wall, J.; Guntert, P.; Bockmann, A.; Glockshuber, R.; Meier, B. H. *Angew. Chem., Int. Ed.* **2015**, *54*, 331−335.
(29) Norlin, N.; Hellberg, M.; Filippov, A.; Sousa, A. A.; Grobner, G.; Leapman, R. D.; Almqvist, N.; Antzutkin, O. N. *J. Struct. Biol.* **2012**, *180*, 174−89.
(30) Colvin, M. T.; Silvers, R.; Ni, Q. Z.; Can, T. V.; Sergeyev, I. V.; Rosay, M.; Donovan, K. J.; Michael, B.; Wall, J. S.; Linse, S.; Griffin, R. G. *J. Am. Chem. Soc.* **2016**, *138*, 9663−9674.
(31) Wälti, M. A.; Ravotti, F.; Arai, H.; Glabe, C. G.; Wall, J. S.; Böckmann, A.; Güntert, P.; Meier, B. H.; Riek, R. *Proc. Natl. Acad. Sci. U. S. A.* **2016**, *113*, E4976−E4984.
(32) Rienstra, C. M.; Tucker-Kellogg, L.; Jaroniec, C. P.; Hohwy, M.; Reif, B.; McMahon, M. T.; Tidor, B.; Lozano-Perez, T.; Griffin, R. G. *Proc. Natl. Acad. Sci. U. S. A.* **2002**, *99*, 10260−10265.
(33) Böckmann, A.; Gardiennet, C.; Verel, R.; Hunkeler, A.; Loquet, A.; Pintacuda, G.; Emsley, L.; Meier, B. H.; Lesage, A. *J. Biomol. NMR* **2009**, *45*, 319−327.
(34) Massiot, D.; Fayon, F.; Capron, M.; King, I.; Le Calve, S.; Alonso, B.; Durand, J. O.; Bujoli, B.; Gan, Z. H.; Hoatson, G. *Magn. Reson. Chem.* **2002**, *40*, 70−76.
(35) Yao, H.; Lee, M. W.; Waring, A. J.; Wong, G. C.; Hong, M. *Proc. Natl. Acad. Sci. U. S. A.* **2015**, *112*, 10926−31.
(36) Wang, T.; Salazar, A.; Zabotina, O. A.; Hong, M. *Biochemistry* **2014**, *53*, 2840−54.
(37) Huster, D.; Yao, X.; Hong, M. *J. Am. Chem. Soc.* **2002**, *124*, 874−83.
(38) Etzkorn, M.; Martell, S.; Andronesi, O. C.; Seidel, K.; Engelhard, M.; Baldus, M. *Angew. Chem., Int. Ed.* **2007**, *46*, 459−462.
(39) Andronesi, O. C.; von Bergen, M.; Biernat, J.; Seidel, K.; Griesinger, C.; Mandelkow, E.; Baldus, M. *J. Am. Chem. Soc.* **2008**, *130*, 5922−8.
(40) Liao, S. Y.; Fritzsching, K. J.; Hong, M. *Protein Sci.* **2013**, *22*, 1623−1638.
(41) Siemer, A. B.; Huang, K. Y.; McDermott, A. E. *Proc. Natl. Acad. Sci. U. S. A.* **2010**, *107*, 17580−5.
(42) Mandal, A.; van der Wel, P. C. *Biophys. J.* **2016**, *111*, 1965−1973.

DOI: 10.1021/jacs.7b02089
J. Am. Chem. Soc. 2017, 139, 6242−6252

(43) Vugmeyster, L.; Clark, M. A.; Falconer, I. B.; Ostrovsky, D.; Gantz, D.; Qiang, W.; Hoatson, G. L. *J. Biol. Chem.* **2016**, *291*, 18484−18495.
(44) Miller, Y.; Ma, B.; Nussinov, R. *J. Am. Chem. Soc.* **2011**, *133*, 2742−2748.
(45) Zheng, J.; Jang, H.; Ma, B.; Tsai, C. J.; Nussinov, R. *Biophys. J.* **2007**, *93*, 3046−3057.
(46) Nicotera, I.; Coppola, L.; Rossi, C. O.; Youssry, M.; Ranieri, G. A. *J. Phys. Chem. B* **2009**, *113*, 13935−13941.
(47) Fichou, Y.; Schirò, G.; Gallat, F. X.; Laguri, C.; Moulin, M.; Combet, J.; Zamponi, M.; Härtlein, M.; Picart, C.; Mossou, E.; Lortat-Jacob, H.; Colletier, J. P.; Tobias, D. J.; Weik, M. *Proc. Natl. Acad. Sci. U. S. A.* **2015**, *112*, 6365−6370.

DOI: 10.1021/jacs.7b02089
J. Am. Chem. Soc. 2017, 139, 6242−6252